

On the Energy Efficiency of MIMO Hybrid Beamforming for Millimeter Wave Systems with Nonlinear Power Amplifiers

Nima N. Moghadam, *Member, IEEE*, Gábor Fodor, *Senior Member, IEEE*, Mats Bengtsson, *Senior Member, IEEE*, and David J. Love, *Fellow, IEEE*

Abstract

Multiple-input multiple-output (MIMO) millimeter wave (mmWave) systems are vulnerable to hardware impairments due to operating at high frequencies and employing a large number of radio-frequency (RF) hardware components. In particular, nonlinear power amplifiers (PAs) employed at the transmitter distort the signal when operated close to saturation due to energy efficiency considerations. In this paper, we study the performance of a MIMO mmWave hybrid beamforming scheme in the presence of nonlinear PAs. First, we develop a statistical model for the transmitted signal in such systems and show that the spatial direction of the inband distortion is shaped by the beamforming filter. This suggests that even in the large antenna regime, where narrow beams can be steered toward the receiver, the impact of nonlinear PAs should not be ignored. Then, by employing a realistic power consumption model for the PAs, we investigate the trade-off between spectral and energy efficiency in such systems. Our results show that increasing the transmit power level when the number of transmit antennas grows large can be counter-effective in terms of energy efficiency. Furthermore, using numerical simulation, we show that when the transmit power is large, analog beamforming leads to higher spectral and energy efficiency compared to digital and hybrid beamforming schemes.

The work of N. N. Moghadam and G. Fodor was partially financed by Ericsson Research through the HARALD project. The work of D. J. Love was supported in part by the National Science Foundation under grant NSF CCF1403458.

N. N. Moghadam and M. Bengtsson are with the School of Electrical Engineering, KTH Royal Institute of Technology, 100 44 Stockholm, Sweden (e-mail: nimanm@kth.se; mats.bengtsson@ee.kth.se).

G. Fodor is with the School of Electrical Engineering, KTH Royal Institute of Technology, 100 44 Stockholm, Sweden, and also with Ericsson Research, 164 83 Kista, Sweden (e-mail: gaborf@kth.se).

D. J. Love is with the School of Electrical and Computer Engineering, Purdue University, West Lafayette, IN 47906 USA (e-mail: djlove@purdue.edu).

I. INTRODUCTION

Large scale multiple-input multiple-output (LS-MIMO) systems involving an order of magnitude greater number of antenna elements than in the early releases of wireless standards are key enablers of next generation mobile broadband services [1]. Theoretically, a fully digital LS-MIMO beamforming architecture employing a large number of digital transmit and receiver chains can yield optimal performance in terms of energy and spectral efficiency [2].

However, deploying LS-MIMO systems in traditional cellular frequency bands is problematic due to the large physical size of the antenna arrays and related environmental concerns of the general public. Therefore, higher frequency bands, including the millimeter-wave (mmWave) bands have recently emerged as an appealing alternative for the commercial deployment of LS-MIMO systems [3]. Indeed, in mmWave bands, the physical array size can be greatly reduced, and, as an additional advantage, vast amount of unused spectrum can be utilized for attractive and bandwidth-demanding services [4], [5].

Deploying a large number of antennas with the associated fully digital beamforming architecture incurs high cost and increased power consumption, due to the excessive demand for a large number of transceiver chains. Therefore, LS-MIMO systems with hybrid analog and digital beamforming for mmWave deployment have attracted much attention from the research and engineering communities, and a great number of promising hybrid architectures and associated technologies such as training sequence and codebook designs have been proposed and tested in practice [6]–[11]. The results of the marriage of LS-MIMO and hybrid beamforming include significant gains in terms of spectral and energy efficiency, and a cost-efficient technology for accessing large amount of unused spectrum [2], [9], [12].

In practice, the performance and scalability of LS-MIMO systems are confined by a variety of hardware limitations and impairments that distort the transmitted and received signals [13]–[16]. The recognition of the importance of analysing and overcoming the impact of non-ideal hardware and, in particular, nonlinear power amplifiers (PAs) on LS-MIMO performance has triggered intensive research resulting in valuable insights.

First, the distortion introduced in the transmit signal by an LS-MIMO transmitter is mainly caused by radio frequency (RF) impairments, such as in-phase/quadrature-phase imbalance, crosstalk, and, predominantly, by high power amplifier (HPA) nonlinearity, especially when HPAs operate close to saturation [14], [17], [18]. Conventionally, applying a large back-off from

the saturation power of a PA has been considered as a solution for decreasing the nonlinear distortion since reducing the transmit power allows the PAs to operate in their linear operating region [19]. A serious disadvantage of this solution is that backing off from the saturation level causes PAs to work less energy efficiently, because the PA's ability to generate RF energy decreases when operating away from the saturation point [20]. Secondly, the negative effect of nonlinear distortion can be mitigated by employing waveforms with low peak-to-average-power ratio (PAPR), because signals with a low PAPR are less sensitive to distortion than signals with higher PAPR. Unfortunately, PAPR reduction typically reduces the spectral efficiency, that can only partially be compensated by increased complexity and cost at the receivers [21].

These two observations imply that there is an inherent trade-off between the targeted energy and spectral efficiency and the distortion generated at the transmitter, as has been investigated in [22]. To find near optimum operating points for LS-MIMO systems built on a hybrid beamforming architecture within the constraints of this trade-off is challenging, and requires an accurate model of the distortions caused by hardware impairments including the non-linearities of PAs.

To this end, a common approach is to represent the spatial properties of the distortion as additive white Gaussian noise (AWGN) signals at different antenna elements [13], [15], [16], [23]–[26]. This model assumes that the distortion signals are independent across the different antenna elements and that the distortion power at each antenna element is a monotonically increasing function of the signal power fed to the corresponding antenna branch. These assumptions hold only after sufficient calibrations and compensations where the combined residual of a wide range of independent hardware impairments give rise to an additive distortion signal. Unfortunately, the AWGN-based distortion signal model may not be appropriate when the distortion is predominantly generated by the transmitter's PAs working close to saturation aiming at high spectral and energy efficiency targets. In particular, as pointed out in [27], the spatial direction of the transmitted distortion is dependent on the spatial direction of the transmitted signal, while the AWGN model fails to capture this dependency.

Therefore, in this paper our main objective is to formulate a model that provides a more precise characterization of the statistical properties of the distortion, than the AWGN-based distortion signal model. We use this model to determine the achievable rate and energy efficiency of LS-MIMO systems built on a hybrid analog-digital architecture and operating in mmWave frequency bands in the presence of nonlinear distortion. The analysis is based on the assumption that the PAs have the same transfer function, for all the transmitter branches. Moreover, in

general we assume that the crosstalk between the antenna branches is negligible due to proper isolation. However, in Section III-B, we extend our model to describe the system impaired with crosstalk as well. In particular, we formulate the problem of maximizing the energy efficiency of this system as an optimization task in the digital and analog precoding matrices subject to sum-power constraints.

The rest of the paper is structured as follows. Section I-A presents a summary of the related work. Section II describes the system model that we used in this paper. In Section III, we derive a model for a nonlinearly amplified signal at a multiantenna transmitter. In this section, we further extend our model to describe the system impaired with crosstalk. Section IV and Section V study the spectral and energy efficiency of the system, respectively. We present simulation results in Section VI, followed by concluding remarks in Section VII.

Notations: Capital bold letters denote matrices and lower bold letters denote vectors. The superscripts \mathbf{X}^* , \mathbf{X}^T , \mathbf{X}^H stand for the conjugate, transpose, transpose conjugate of \mathbf{X} , respectively. $[\mathbf{X}]_{ij}$ is the entry of \mathbf{X} at row i and column j . $|x|$ is the absolute value of x . $\mathbf{X} \odot \mathbf{Y}$ denotes the Hadamard (entry-wise) product of matrices \mathbf{X} and \mathbf{Y} . \mathbf{I}_x is an $x \times x$ identity matrix and $\text{diag}(\mathbf{x})$ is a diagonal matrix with entries of \mathbf{x} on its principal diagonal. The set of positive semi-definite (PSD) matrices of size n is denoted by \mathbb{S}^n and \mathbb{R}^+ represents the set of nonnegative real numbers.

A. Related Works and Contributions of the Present Paper

1) *Papers Analyzing the Combined Effects of Hardware Impairments:* A large body of research has investigated the aggregate impacts of RF hardware impairments on the performance of multiple-input multiple-output (MIMO) systems, see for example [13], [15], [16], [20], [24], [26], [28]–[30]. The effects of transmit-receive hardware impairments on the capacity of the MIMO channel and, in particular, MIMO detection algorithms are studied in [13]. This analysis is based on an independent and identically distributed (i.i.d.) Gaussian model for the distortion caused by the hardware impairments. The system-level implications of residual transmit-RF impairments in MIMO systems are studied in [15] using a similar modeling approach as in [13]. In [28], it is shown that the physical MIMO channel has a finite upper capacity limit for any channel distribution and signal-to-noise ratio (SNR), while the results in [24] indicate that the hardware impairments create finite ceilings on the channel estimation accuracy and on the downlink/uplink capacity of each served user equipment (UE) in cellular MIMO systems. The

aggregate effects of hardware imperfections including phase-noise, non-linearities, quantization errors, noise amplification and inter-carrier interference are formulated as practical hardware scaling laws in [29], which proposes circuit-aware design of LS-MIMO systems. In [30], an information theoretic approach is used in order to bound the capacity of a point-to-point single-antenna system, with nonlinearities at both transmitting and receiving sides.

Multicell coordinated beamforming algorithms in the presence of the aggregate effects of hardware impairments are studied in [16] and [26]. These works suggest that impairments-aware beamforming algorithms and resource allocation are feasible and yield superior performance as compared with algorithms that assume ideal hardware.

2) *Papers Focusing on Dominant Impairment Effect:* The nonlinearity of high power RF amplifiers is often the predominant hardware impairment and has a crucial effect on the performance of MIMO systems, as was emphasized in [14], [18], [31], which characterize the effect of memoryless nonlinear hardware on the performance of MIMO systems. In particular, [14] investigated the performance of MIMO orthogonal space-time block coding systems in the presence of nonlinear high-power amplifiers (HPAs), and proposed a sequential Monte Carlo-based compensation method for the HPA nonlinearity. Subsequently, the optimal transmit beamforming scheme in the presence of nonlinear HPAs is found in [18] using a general nonlinearity model for the transmitter RF-chains. However, the suggested strategy is not practical as the precoders depend on the transmitted signal and hence need to be designed prior to each channel use. Furthermore, an accurate knowledge about the nonlinearity model of the transmitters is needed, which makes the design of the precoders complicated.

More recently, the inherent trade-off between nonlinearity distortions and power efficiency was studied in [31]. That paper uses a polynomial model for the transmitter PAs, and – following the approach in [20] for modeling the nonlinear distortion – derived the ergodic rate for MIMO systems.

3) *Papers Dealing with mmWave Systems:* Specifically, in the framework of mmWave communications, [32]–[34] have studied the effect of hardware impairments on the performance of MIMO systems. The results of [32] show that single-carrier frequency domain equalization is more robust against impairments from nonlinear power amplifiers than orthogonal frequency division multiplexing (OFDM) in typical mmWave system configurations. On the other hand, the results reported in [33] show a slight bit error rate performance advantage of OFDM over single-carrier frequency domain equalization under nonlinear RF distortions, and suggest that

subcarrier spacing is a crucial parameter in mmWave massive MIMO systems.

4) *Papers Related to Power Minimization and Energy Efficiency:* References [29], [35], [36] provide insights related to the energy efficiency of MIMO systems. Reference [35] proposes a PA-aware power allocation scheme that takes into account the power dissipation at the PAs in MIMO systems, and results in substantial gains in terms of data rate and consumed power compared with non-PA-aware power allocation schemes. Subsequently, a low computational complexity algorithm that finds the minimum consumed power for any given mutual information is developed in [36]. This algorithm gives significant rate and total consumed power gains in comparison with non-PA-aware algorithms. Energy efficient optimal designs of multi-user MIMO systems are developed in [29], where the number of antennas, active (scheduled) users and transmit power levels are part of the design and operation parameters. However, in this latter paper the impact of hardware impairments are not taken into account. Additionally, the impact of regulatory electromagnetic exposure constraints has also been taken into account when designing multiple transmit antenna signals in [37]–[39]. Recently, the interplay between waveforms, amplifier efficiency, distortion and performance in the massive MIMO downlink was studied in [40]. In that work, it was found that in terms of the consumed power by the PAs, OFDM and single-carrier transmission have similar performance over the hardened massive MIMO channel, and low-PAPR precoding at massive MIMO base stations can significantly increase the power efficiency as compared with PAPR-unaware precoders.

5) *Contributions of the Present Paper:* In this paper, we consider a multi-antenna transmit signal model that incorporates the distortion generated by each PA. Under the assumption that the PAs in the different antenna branches have the same input-output relation and follow a memoryless polynomial model, we show that the nonlinear distortion vector is a zero mean complex random vector and derive its covariance matrix in closed form. Since the resulting statistics of the nonlinear distortion vector is a function of the covariance matrix of the beamformed signal, it is therefore affected by the transmit beamforming filters. Next, for the special case of a single RF chain, we derive a closed form expression both for the maximum spectral efficiency and for a lower bound on the achievable rate. We then consider the problem of optimizing the energy efficiency of the system as a function of the consumed power per information bit using a realistic power consumption model for the transmit PAs.

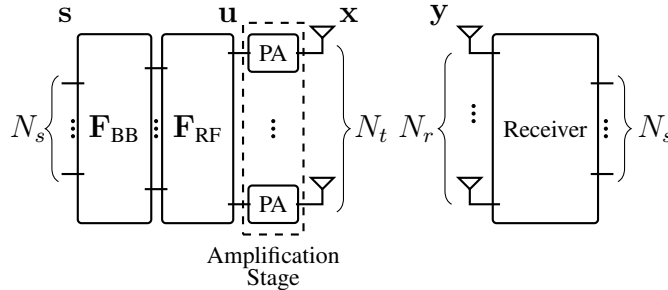


Fig. 1: System model.

II. SIGNAL AND SYSTEM MODEL

A. System Model

Consider a single-carrier mmWave system where a transmitter with N_t antennas and $N_{\text{RF}} \ll N_t$ RF-chains communicates with a receiver equipped with N_r antennas. We assume that the receiver is equipped with N_r RF-chains and has an all-digital structure. The transmitter is intended to convey a complex symbol vector denoted by $\mathbf{s} \sim \mathcal{CN}(\mathbf{0}, \mathbf{I}_{N_s})$ to the receiver, where $N_s \leq N_{\text{RF}}$ is the number of transmitted streams. The symbol is beamformed in the baseband by a beamforming matrix $\mathbf{F}_{\text{BB}} \in \mathbb{C}^{N_{\text{RF}} \times N_s}$ and in the analog domain using a network of phase-shifters with transfer matrix $\mathbf{F}_{\text{RF}} \in \mathbb{C}^{N_t \times N_{\text{RF}}}$. Therefore, the beamformed signal is $\mathbf{u} = [u_1, \dots, u_{N_t}]^T \doteq \mathbf{F}_{\text{RF}} \mathbf{F}_{\text{BB}} \mathbf{s} \in \mathbb{C}^{N_t}$ and is distributed as $\mathcal{CN}(\mathbf{0}, \mathbf{C}_{\mathbf{u}})$, where

$$\mathbf{C}_{\mathbf{u}} \doteq \mathbb{E} \{ \mathbf{u} \mathbf{u}^H \} = \mathbf{F}_{\text{RF}} \mathbf{F}_{\text{BB}} \mathbf{F}_{\text{BB}}^H \mathbf{F}_{\text{RF}}^H \in \mathbb{C}^{N_t \times N_t}. \quad (1)$$

The beamformed signal then goes through the amplification stage, where at each antenna branch a PA, with transfer function $f(\cdot)$, amplifies the signal before transmission. We will elaborate further on the function $f(\cdot)$ in Section II-B. We represent the transmitted signal collectively by $\mathbf{x} \doteq [f(u_1), \dots, f(u_{N_t})]^T$, where we have assumed that all the PAs have the same transfer function and there is no coupling between the different antenna branches. Therefore, the received signal is

$$\mathbf{y} = \mathbf{H} \mathbf{x} + \mathbf{n} \in \mathbb{C}^{N_r}, \quad (2)$$

where $\mathbf{H} \in \mathbb{C}^{N_r \times N_t}$ represents the channel and $\mathbf{n} \sim \mathcal{CN}(\mathbf{0}, \sigma_n^2 \mathbf{I}_{N_r})$ is the receiver thermal noise. Fig. 1 illustrates the system model¹.

¹ The transmitter structure used in this paper is also suggested in several other works including [2], [8], [41].

B. PA Model

Behavioural modeling of PAs using polynomials is a low-complexity, mathematically tractable and yet accurate method which has long been used in the RF PA design literature (see, e.g., [20], [42], [43]). Accordingly, in this paper we adapt a memoryless polynomial model of order $2M + 1$ to describe the nonlinear behavior of the transmitter PAs. Note that by adjusting the model parameters, this model can provide an arbitrarily exact approximation of any other well-known (memoryless) models that has been introduced for PAs in the literature (e.g., see [20, Chapter 6]). Clearly, the dynamic behavior of a PA due to its memory effect is not captured in the memoryless polynomial model, and the investigation of this effect on the performance of the system is out of the scope of this work².

Furthermore, we assume that the PAs in the different antenna branches follow the same input-output relation. This assumption is widely used in the literature [20], [40], [44]. In this case, the equivalent baseband output signal of the n^{th} PA is

$$x_n = f(u_n) \doteq \sum_{m=0}^M \beta_{2m+1} |u_n|^{2m} u_n, \quad (3)$$

where β_{2m+1} 's are the model parameters and take complex values in general. Usually, only a limited number of terms in this model suffices for modeling the *smooth* nonlinear PAs at the RF front-ends. Observe that in this model the even order terms are omitted as they only contribute to the out-of-band distortion and lead to spectrum regrowth [20].

Using (3), we define the instantaneous (amplitude) gain of the n^{th} PA as

$$g_n \doteq \frac{x_n}{u_n} = \sum_{m=0}^M \beta_{2m+1} |u_n|^{2m}. \quad (4)$$

This equation implies that both the absolute value and phase of the PA's instantaneous gain depends on the input signal's amplitude $|u_n|$. In the literature, the effect of the signal's amplitude on the absolute value and phase of the PA's gain are referred to as amplitude-to-amplitude (AM-AM) and amplitude-to-phase (AM-PM) characteristics of the PA, respectively. In practical PAs, the AM-AM is a monotonically decreasing function³ of the input's amplitude while the AM-PM is only slightly changing at high amplitudes.

²The dynamic behaviour of PAs has been considered in some of the previous works such as [34].

³Note that although the AM-AM gain of a PA is a monotonically decreasing function of the input amplitude, the output amplitude increases with the input signal's amplitude.

C. Channel Model

We consider a cluster channel model [6] with L paths between the transmitter and the receiver. Let ψ_ℓ denote the complex gain of path ℓ between the transmitter and the receiver, which includes both the path-loss and small-scale fading. In particular, for the given large-scale fading, $\{\psi_\ell\}$ for all $\ell \in \{1, \dots, L\}$ are i.i.d. random variables drawn from distribution $\mathcal{CN}(0, 10^{-0.1\text{PL}})$ where PL is the path-loss in dB [45]. The path-loss consists of a constant attenuation, a distance dependent attenuation, and a large scale log-normal fading. The channel matrix between the transmitter and the receiver is

$$\mathbf{H} = \sqrt{\frac{N_t N_r}{L}} \sum_{\ell=1}^L \psi_\ell \mathbf{a}_r(\theta_\ell) \mathbf{a}_t^H(\phi_\ell) = \mathbf{A}_r \mathbf{\Psi} \mathbf{A}_t^H \in \mathbb{C}^{N_r \times N_t}, \quad (5)$$

where θ_ℓ and ϕ_ℓ are the angle of arrival (AoA) and angle of departure (AoD) corresponding to path ℓ of the channel, respectively. Vectors $\mathbf{a}_t \in \mathbb{C}^{N_t}$ and $\mathbf{a}_r \in \mathbb{C}^{N_r}$ represent the unit-norm array response vectors of the transmitter and the receiver antenna arrays, respectively, $\mathbf{A}_t = [\mathbf{a}_t(\phi_1), \dots, \mathbf{a}_t(\phi_L)]$, $\mathbf{A}_r = [\mathbf{a}_r(\theta_1), \dots, \mathbf{a}_r(\theta_L)]$, and $\mathbf{\Psi} \in \mathbb{C}^{L \times L}$ is a diagonal matrix whose ℓ -th diagonal entry is $\psi_\ell = \sqrt{N_t N_r / L}$. We assume that both of the transmitter and the receiver are equipped with uniform linear arrays (ULAs) with array responses

$$\mathbf{a}_t(\phi) = \frac{1}{\sqrt{N_t}} [1, e^{-j2\pi D_t \sin(\phi)}, \dots, e^{-j2\pi(N_t-1)D_t \sin(\phi)}]^T, \quad (6)$$

$$\mathbf{a}_r(\theta) = \frac{1}{\sqrt{N_r}} [1, e^{-j2\pi D_r \sin(\theta)}, \dots, e^{-j2\pi(N_r-1)D_r \sin(\theta)}]^T, \quad (7)$$

where D_t and D_r represent the antenna spacing of the transmitter and receiver, respectively, normalized to the carrier wavelength.

III. NONLINEAR POWER AMPLIFICATION

A. Nonlinear Distortion

Due to the nonlinear behaviour of the PAs in the amplification stage, the transmitted signal is an amplified and distorted version of the input signal, \mathbf{u} . On the one hand, using the PA model of Section II-B, the transmitted signal is a function of \mathbf{u} as represented in $\mathbf{x} = [f(u_1), \dots, f(u_{N_t})]^T$, where $f(\cdot)$ is defined in (3). On the other hand, following the approach in [46] and extending it to the multiantenna case, the same signal can be represented as a linearly amplified version of the input signal \mathbf{u} contaminated with the nonlinear distortion. That is

$$\mathbf{x} = \bar{\mathbf{G}} \mathbf{u} + \mathbf{d} \in \mathbb{C}^{N_t}, \quad (8)$$

where $\bar{\mathbf{G}}$ denotes the average linear gain of the amplification stage and $\mathbf{d} = [d_1, \dots, d_{N_t}]^T$ in which d_n is the distortion generated by the n^{th} PA. According to the definition in [46], the distortion generated at the output of each PA is uncorrelated with the input signal to that PA, i.e., $\mathbb{E}\{u_n^* d_n\} = 0$ for $n = 1, \dots, N_t$. Subsequently, we can conclude that $\mathbb{E}\{u_n^* d_k\} = 0$ for any $k, n \in \{1, \dots, N_t\}$. Furthermore, we assume that the antenna branches are perfectly isolated from each other and therefore the coupling between them is negligible. Hence, $\bar{\mathbf{G}}$ is assumed to be a diagonal matrix.

By collectively representing the instantaneous gain of the power amplification stage by $\mathbf{G} = \text{diag}(g_1, \dots, g_{N_t})$, the transmitted signal can be alternatively represented as $\mathbf{x} = \mathbf{G}\mathbf{u}$. Correspondingly, by substituting $\mathbf{x} = \mathbf{G}\mathbf{u}$ into (8), the nonlinear distortion can be expressed as

$$\mathbf{d} = (\mathbf{G} - \bar{\mathbf{G}})\mathbf{u}. \quad (9)$$

Let us denote the average power of the input signal to the n^{th} PA by $P_n \doteq \mathbb{E}\{|u_n|^2\} = [\mathbf{C}_{\mathbf{u}}]_{nn}$, the following two propositions characterize the average linear gain and the nonlinear distortion signal.

Proposition 1. *The average linear gain $\bar{\mathbf{G}}$ of the power amplification stage in (8) is*

$$\bar{\mathbf{G}} = \text{diag}(\bar{g}(P_1), \dots, \bar{g}(P_{N_t})) , \quad (10)$$

where $\bar{g}(P_n) = \sum_{m=0}^M \beta_{2m+1} P_n^m (m+1)!$.

A sketch of proof for Proposition 1 is given in the Appendix.

Proposition 2. *The nonlinear distortion vector \mathbf{d} in (8) is a zero-mean complex random vector with covariance matrix*

$$\mathbf{C}_{\mathbf{d}} = \sum_{m=1}^M \Gamma_m \overbrace{(\mathbf{C}_{\mathbf{u}} \odot \dots \odot \mathbf{C}_{\mathbf{u}})}^{(m+1) \text{ times}} \odot \overbrace{(\mathbf{C}_{\mathbf{u}}^T \odot \dots \odot \mathbf{C}_{\mathbf{u}}^T)}^{m \text{ times}} \Gamma_m^H, \quad (11)$$

where $\Gamma_m = \text{diag}(\gamma_m(P_1), \dots, \gamma_m(P_{N_t}))$ and

$$\gamma_m(P_n) = \sqrt{\frac{1}{m+1}} \sum_{q=m}^M \beta_{2m+1} \binom{q}{m} (q+1)! P_n^{(q-m)}. \quad (12)$$

Proof: A proof is given in the Appendix. □

As Proposition 2 implies, the spatial direction of the nonlinear distortion is dependent on the direction of the beamformed signal. Therefore, an important intuition from this proposition is

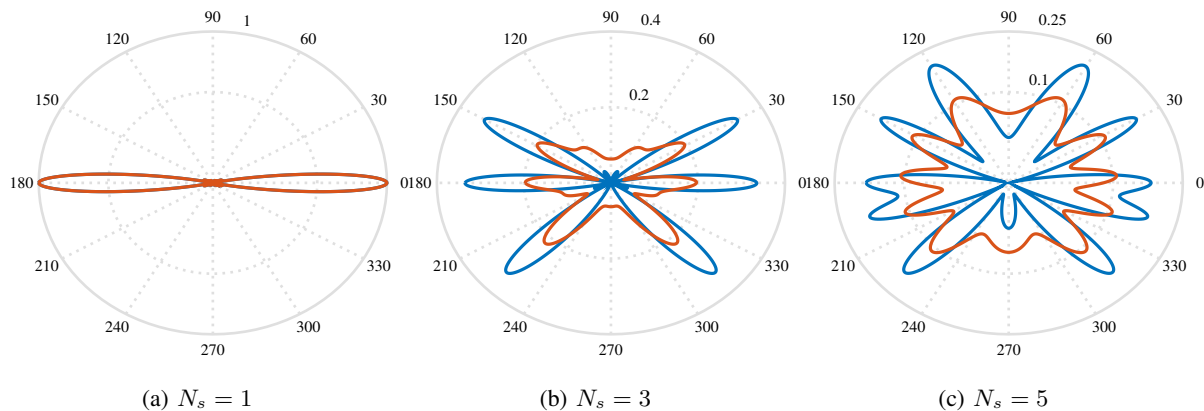


Fig. 2: Normalized beam pattern of the radiated desired signal (blue) and the radiated distortion signal (red). Note that when only one stream is transmitted, i.e. $N_s = 1$, distortion and desired signal have the same beam pattern.

that by beamforming the desired signal, the distortion is also beamformed toward the receiver. As we will see in the next sections, this phenomenon affects the spectral and energy efficiency of the system, especially when the PAs are pushed to work in their energy efficient, but nonlinear, regions. The following example elaborates further on this intuition.

Example 1. Consider a mmWave system as described in Section II with $N_t = 8$ and the PA model parameters stated in Table I. Assume that $N_s = N_{RF}$ and no baseband beamforming is applied, i.e., $\mathbf{F}_{BB} = \frac{1}{\sqrt{N_s}}\mathbf{I}_{N_s}$. Figure 2 illustrates the simulated beam pattern of the transmitted signal when the analog beamformer $\mathbf{F}_{RF} = [\mathbf{a}_t(\phi_1), \dots, \mathbf{a}_t(\phi_{N_s})]$ is used for $N_s = 1, 3, 5$. In this figure, the AoDs, i.e. ϕ_i , $i = 1, \dots, 5$, are $0, -\pi/4, \pi/6, \pi/3, -\pi/12$, respectively. As the figure implies, the peak power of the distortion signal is steered in the same direction as the desired beamformed signal. However, as the number of transmitted streams increases, the distortion signal behaves more like an omnidirectional noise. Mathematically, we can also see that as the number of transmitted streams from antenna branches increase, the off-diagonal elements of \mathbf{C}_d get smaller compared to the diagonal elements.

In the case where $N_s < N_{RF}$ and the signal is digitally beamformed in the baseband, the effect of N_s on the directionality of radiated distortion signal is not easily tractable. In general, the directionality of the distortion signal depends on the hybrid beamformer $\mathbf{F}_{RF}\mathbf{F}_{BB}$, and subsequently on \mathbf{C}_u , as Proposition 2 implies. This proposition shows that as the beamformed signals transmitted from different antenna branches become more uncorrelated (i.e., the off-

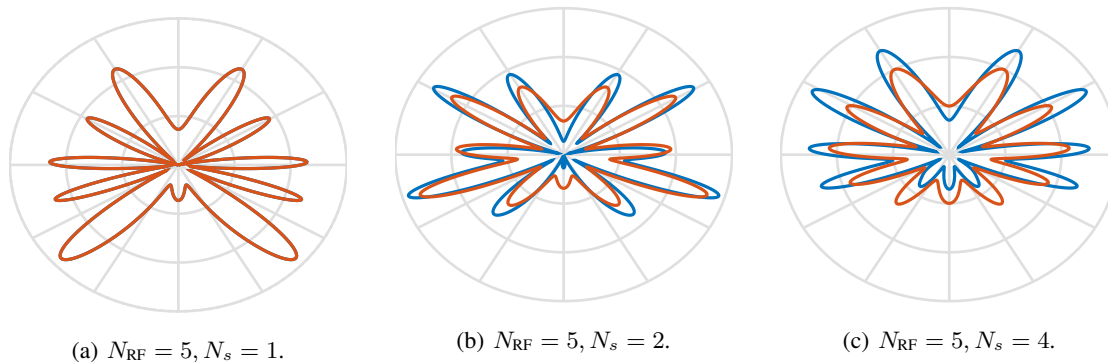


Fig. 3: Normalized beam pattern of the radiated desired signal (blue) and the radiated distortion signal (red). Note that when only one stream is transmitted, i.e. $N_s = 1$, distortion and desired signal have the same beam pattern.

diagonal elements of \mathbf{C}_u become smaller), the distortion behaves more like an omni-directional signal with almost equal power transmitted in different directions. Below, we show the effect of N_s on the radiated distortion in a simple example.

Example 2. Consider the system of Example 1 where $N_s < N_{RF}$ streams are beamformed using a hybrid beamformer $\mathbf{F}_{RF}\mathbf{F}_{BB}$. Fig. 3 illustrates the simulated beam pattern of the transmitted desired signal as well as the radiated distortion for different numbers of streams, N_s , when $N_{RF} = 5$. In this figure, the entries of \mathbf{F}_{BB} are i.i.d. Gaussian distributed. As the figure shows, when $N_s = 1$ (and consequently all the signals transmitted from different antennas are fully correlated) then the distortion signal is transmitted in the direction of desired signal, similarly to Example 1. However unlike Example 1, increasing N_s from 2 to 4 while keeping N_{RF} constant does not necessarily lead to lower directionality in the distortion signal.

B. Nonlinear Crosstalk

Another impairment that is observed in multi-antenna systems is *crosstalk*, which is due to coupling of the signal from one antenna branch to another. If we make the assumption that the antenna branches are sufficiently isolated from each other, the coupling can be modeled as a linear crosstalk between different antenna branches [47]. The linear coupling of the signals after the amplification stage can in principle be seen as part of the channel and therefore is not studied separately in this paper. However, the coupling before the amplification stage results in a nonlinear crosstalk impairment. In this case, the input signal to the amplification stage will be

$$\tilde{\mathbf{u}} = \mathbf{B}_{TX}\mathbf{u}, \quad (13)$$

where $\mathbf{B}_{\text{TX}} \in \mathbb{C}^{N_t \times N_t}$ represents the transmit coupling matrix. Moreover, when coupling exists, both the average linear gain $\bar{\mathbf{G}}$ and the distortion vector \mathbf{d} will be affected by the coupling matrix through the covariance matrix of $\tilde{\mathbf{u}}$ which is

$$\mathbf{C}_{\tilde{\mathbf{u}}} = \mathbb{E} \{ \mathbf{B}_{\text{TX}} \mathbf{u} \mathbf{u}^H \mathbf{B}_{\text{TX}}^H \} = \mathbf{B}_{\text{TX}} \mathbf{C}_{\mathbf{u}} \mathbf{B}_{\text{TX}}^H. \quad (14)$$

Replacing $P_n = [\mathbf{C}_{\mathbf{u}}]_{nn}$ by $\tilde{P}_n = [\mathbf{C}_{\tilde{\mathbf{u}}}]_{nn}$, $n = 1, \dots, N_t$ in (10) and (12) and replacing $\mathbf{C}_{\mathbf{u}}$ by $\mathbf{C}_{\tilde{\mathbf{u}}}$ in (11) gives the average linear gain, $\tilde{\mathbf{G}}$, and the covariance of the distortion signal, $\mathbf{C}_{\tilde{\mathbf{d}}}$, in systems with coupling.

In the sequel, we ignore the crosstalk impairment and focus on the effects of the distortion on the system performance unless otherwise stated. In the next section, we investigate the performance of the system in terms of achievable rate and the consumed power per information bit.

IV. SPECTRAL EFFICIENCY

The distortion signal is a self-interference which is generated by the desired signal itself. Therefore, it carries information about the desired signal. Nonetheless, extracting information from it relies on two impractical conditions. First, a precise knowledge about the nonlinear behavior of the system should be available. Second, a complicated nonlinear receiver should be employed. In practice, it is easier to treat the received distortion as noise and discard the information buried in it. Furthermore, the received distortion is not necessarily Gaussian distributed. However, by noticing that among different distributions of the additive noise, the Gaussian distribution leads to the smallest possible spectral efficiency [48], we define the (worst case) spectral efficiency of the system (in bits/sec/Hz) as

$$SE \doteq \log_2 \det \left(\mathbf{I}_{N_r} + (\mathbf{H} \mathbf{C}_{\tilde{\mathbf{d}}} \mathbf{H}^H + \sigma_n^2 \mathbf{I}_{N_r})^{-1} \mathbf{H} \tilde{\mathbf{C}}_{\mathbf{u}} \mathbf{H}^H \right), \quad (15)$$

where $\tilde{\mathbf{C}}_{\mathbf{u}} \doteq \bar{\mathbf{G}} \mathbf{C}_{\mathbf{u}} \bar{\mathbf{G}}^H$ is the covariance matrix of the transmitted desired signal. Note that the spectral efficiency in (15) gives a lower-bound on the capacity of the nonlinear channel, since part of the transmitted information is regarded as undesired distortion at the receiver. The following proposition gives the maximum spectral efficiency, optimized over the beamforming vector \mathbf{F}_{RF} , for the special case where the transmitter is equipped with one RF chain.

Proposition 3. *In the case where $N_{RF} = 1$, the maximum spectral efficiency of the system described in Section II, maximized over the beamforming vector \mathbf{F}_{RF} , is*

$$\overline{SE} = \log_2 \det \left(\mathbf{I}_{N_r} + \left(\tilde{\mathbf{H}} \tilde{\mathbf{H}}^H \bar{g}_d \left(\frac{P}{N_t} \right) + \frac{\sigma_n^2}{P} \right)^{-1} \tilde{\mathbf{H}} \tilde{\mathbf{H}}^H \bar{g}_s \left(\frac{P}{N_t} \right) \right), \quad (16)$$

where $P \doteq \mathbb{E}\{\|\mathbf{u}\|^2\} = \sum_{n=1}^{N_t} P_n$ is the total input power into the amplification stage, $\tilde{\mathbf{H}} \doteq 1/\sqrt{N_t} \mathbf{H} \mathbf{a}_t(\phi_{\max})$ is the effective channel between the transmitter and the receiver, ϕ_{\max} is the AoD corresponding to the path with the largest small scale fading gain, and

$$\bar{g}_s(P/N_t) \doteq |\bar{g}(P/N_t)|^2, \quad (17)$$

$$\bar{g}_d(P/N_t) \doteq \sum_{m=1}^M |\gamma_m(P/N_t)|^2 (P/N_t)^{2m}. \quad (18)$$

Proof: A proof is given in the Appendix. □

Corollary 1. *A lower-bound on the achievable rate of the system described in (2) when $N_{RF} = 1$ can be found as*

$$\overline{SE} \geq \log_2 \left(1 + \frac{\bar{g}_s \left(\frac{P}{N_t} \right)}{\bar{g}_d \left(\frac{P}{N_t} \right) + \frac{\sigma_n^2}{\delta P}} \right). \quad (19)$$

where $\delta = |1/\sqrt{N_t N_r} (\mathbf{a}_r(\theta_{\max}))^H \mathbf{H} \mathbf{a}_t(\phi_{\max})|^2$ is the effective channel gain and θ_{\max} is the AoA corresponding to the path with the largest small scale fading gain. This bound is tight when $L = N_{RF}$.

The proof of Corollary 1 is a straightforward application of Lemma 4 in the Appendix.

Corollary 1 clearly shows that the benefit of increasing the number of transmit antennas N_t on the spectral efficiency of the system is two-fold. On one hand, by coherently transmitting the signal, an array gain proportional to N_t can be obtained. This gain is reflected in the effective channel gain δ . On the other hand, the input signal power to each PA decreases inversely with N_t which leads to a higher linear gain for the desired signal and lower distortion power.

V. ENERGY EFFICIENCY

Spectrally efficient modulation techniques, such as OFDM, lead to signals with a high PAPR, which are more prone to the distortion, specially when the PAs in the amplification stage are working close to saturation. One conventional technique to avoid distortion is to apply a large input back-off (IBO) at the input of the PAs. By applying IBO, the input powers are decreased

to ensure that the PAs are operating in their linear region even when the signals are at their peaks.

Although the smaller input power leads to less distortion at the output of a PA, reducing the input power at the same time decreases the power efficiency of the PA leading to more power dissipation in the system. In fact, there is a trade-off between the spectral and energy efficiency of the system on one side and the generated distortion on the other side [22]. In order to investigate this trade-off in our system, we first need to find the total power consumption of the system.

Let us denote the power efficiency of the n^{th} PA by

$$\eta(P_n) \doteq \frac{P_{\text{rad},n}}{P_{\text{cons},n}}, \quad (20)$$

where $P_{\text{rad},n} \doteq [\tilde{\mathbf{C}}_{\mathbf{u}}]_{nn} + [\mathbf{C}_{\mathbf{d}}]_{nn}$ is the radiated power from the n^{th} antenna and $P_{\text{cons},n}$ is the consumed power by the PA including both the radiated power and the dissipated power. Note that not all the radiated power from the antenna is useful at the receiver as part of it belongs to the transmitted distortion signal. Following the approach in [36], the consumed power by the n^{th} PA can be expressed as

$$P_{\text{cons},n} = \frac{\sqrt{P_{\text{max}}}}{\eta_{\text{max}}} \sqrt{P_{\text{rad},n}}, \quad (21)$$

where P_{max} is the maximum output power and η_{max} is the maximum efficiency of the PA. Therefore the total power consumption⁴ is $P_{\text{cons}} \doteq \sum_{n=1}^N P_{\text{cons},n}$.

Remark 1. *Although the maximum efficiency that a PA can achieve is constant and depends on its physical structure, the efficiency of a PA is changing with its input power. In some works such as [2], [29], the efficiency of the transceiver PAs is assumed to be constant and independent from the input power. This can potentially lead to an inaccurate calculation of the consumed power and consequently the energy efficiency of the overall system.*

To characterize the actual energy that is used to transmit one information bit from the transmitter to the receiver we define the energy efficiency of the system (in bits/Joul) as

$$EE \doteq \frac{BW \times SE}{P_{\text{cons}}}, \quad (22)$$

⁴ Since the focus of this paper is on the impact of nonlinear PAs on the system performance, by considering that a large portion of the consumed power in communication systems is used by PAs, we do not include the power consumed by other components in our calculations.

where BW is the total bandwidth of the system used for data transmission. Using (22), the optimal beamforming strategy for maximizing the energy efficiency of system can be found by solving the following problem:

$$\begin{aligned} & \underset{\mathbf{F}_{\text{BB}}, \mathbf{F}_{\text{RF}}}{\text{maximize}} && EE && \text{(P1)} \\ & \text{subject to} && P_{\text{cons}} \leq P_0 \\ & && |[\mathbf{F}_{\text{RF}}]_{i,j}| = \sqrt{1/N_t}, \quad \forall i, j. \end{aligned}$$

The Problem P1 is not convex and is not likely to be solvable in polynomial time. However, in the special case when $N_{\text{RF}} = 1$, the dimension of Problem (P1) reduces to one. Therefore, in this case the problem is tractable and can be solved using numerical approaches. By studying this special case, we can gain some insight into the impact of the input power on the spectral and energy efficiency of the system (see Fig. 5, 6 and 7 for a quick insight). The following proposition gives the equivalent problem of (P1) when $N_{\text{RF}} = 1$.

Proposition 4. *In the case where $N_{\text{RF}} = 1$, Problem (P1) is equivalent to the following problem:*

$$\begin{aligned} & \underset{P}{\text{maximize}} && \overline{SE}/\overline{P}_{\text{cons}} && \text{(P2)} \\ & \text{subject to} && \overline{P}_{\text{cons}} \leq P_0 \end{aligned}$$

where \overline{SE} is given by Proposition 3 and

$$\overline{P}_{\text{cons}} = \frac{\sqrt{P_{\text{max}}}}{\eta_{\text{max}}} \sqrt{\left(\overline{g}_s \left(\frac{P}{N_t} \right) + \overline{g}_d \left(\frac{P}{N_t} \right) \right) P N_t} \quad \text{(23)}$$

Proof: A proof is given in Appendix. □

Note that (P2) has only one dimension and can efficiently be solved in practice by using, for example, the Newton-Raphson method.

VI. NUMERICAL RESULTS

In this section, we present simulation results for a MIMO mmWave system with $N_r = 16$ receiving antennas, and a variable number of transmit antennas. The transmitter and receiver are 15 meters apart. We assume that the number of paths between the transmitter and receiver is $L = 5$. In Fig. 4-7, both the transmitter and the receiver are equipped with $N_{\text{RF}} = 1$ RF chain, while in Fig. 8 the number of RF chains is $N_{\text{RF}} = 5$. The rest of the (fixed) simulation parameters are presented in Table I.

TABLE I: Fixed Parameters in the Numerical Evaluation.

Parameters	Values
Carrier Frequency / Bandwidth	73 GHz / 1 GHz
Noise Power (8 dB noise figure)	-105 dBm
Small Scale Fading Distribution	$\mathcal{CN}(0, 1)$
Large Scale Fading (dB)	$\zeta \sim \mathcal{CN}(0, 8)$
Path Loss (dB) at Distance d (m) NLOS [45]	$86.6 + 24.5 \log_{10}(d) + \zeta$
PA Model Parameters [49]	$\beta_1 = 2.96$ $\beta_3 = 0.1418e^{-j2.816}$ $\beta_5 = 0.003e^{j0.39}$
Maximum PA Efficiency η_{\max}	0.3
Maximum PA Output Power P_{\max}	6 dBm

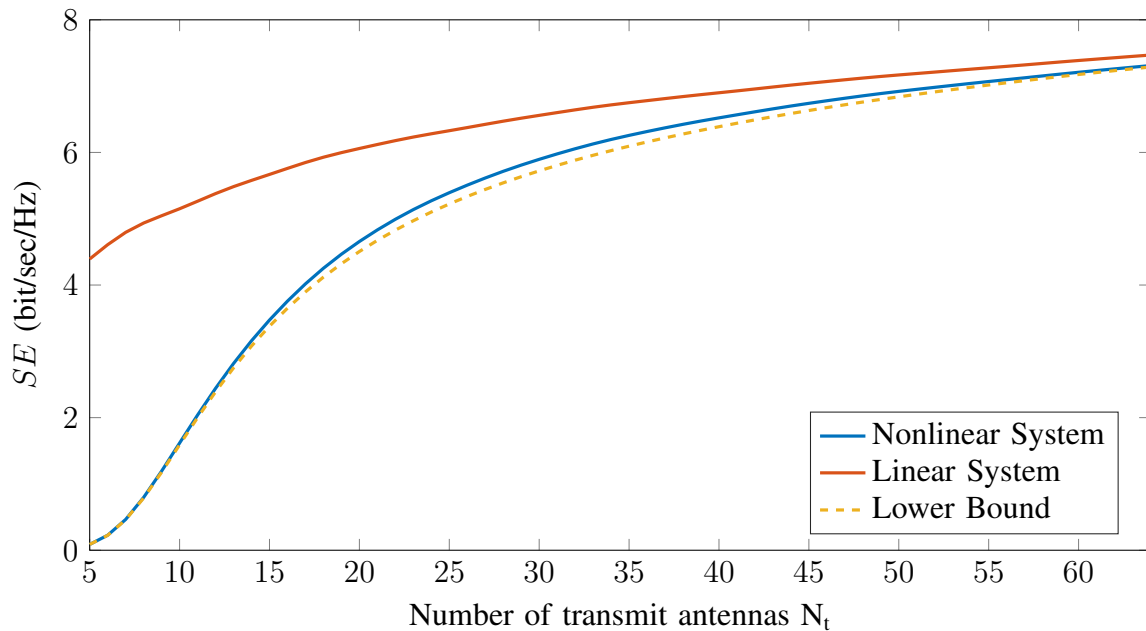


Fig. 4: Spectral efficiency as a function of the number of transmit antennas. In the Nonlinear System the PAs follow a memoryless polynomial model with the parameters stated in Table I. In the Linear System, PAs are linear.

Fig. 4 illustrates the system spectral efficiency as a function of the number of transmit antennas. In this figure, the total input power to the amplification stage, P , is 10 dBm and is fixed for different values of N_t . In this case, $\mathbf{F}_{BB} = 1$ and only an analog beamforming \mathbf{F}_{RF} designed using Proposition 3 is applied at the transmitter.

This figure also shows the maximum spectral efficiency of the system with linear PAs (i.e.,

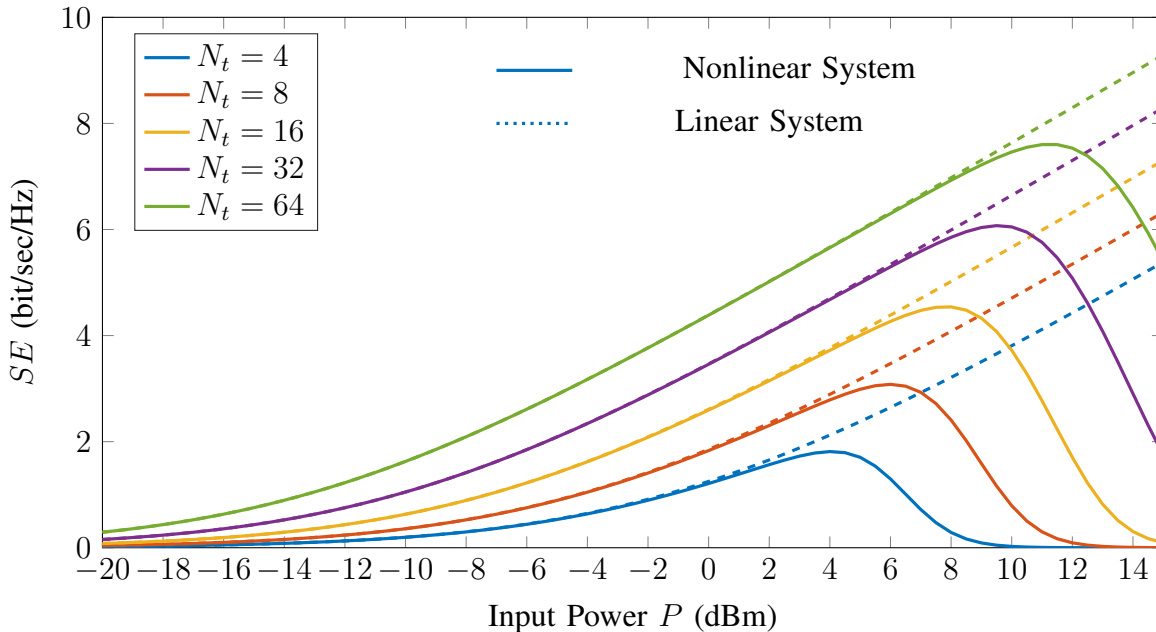


Fig. 5: Spectral efficiency as a function of the input power to the amplification stage. In the Nonlinear System the PAs follow a memoryless polynomial model with the parameters stated in Table I. In the Linear System, PAs are linear.

when $\beta_{2m+1} = 0, \forall m > 0$). In addition, the lower bound found in Corollary 1 is also plotted in this figure. As the figure indicates, by increasing the number of transmit antennas, due to the increase in the array gain, the spectral efficiency of both the linear and nonlinear systems improve. However, this improvement is steeper for the nonlinear system, especially when the number of antennas is small. This happens because assuming a fixed transmit power budget, when N_t is small, the input power to each PA is larger, and consequently the PAs are pushed harder toward saturation, which leads to more distortion radiation from the transmitter. The amount of generated distortion decreases as the input powers decrease and the PAs move toward the linear region.

Fig. 5 shows the spectral efficiency of the system as a function of input power P for different numbers of transmit antennas. In this figure, the same simulation parameters as the ones in Fig. 4, are used. As the figure suggests, the spectral efficiency in nonlinear systems is not a strictly increasing function of the transmit power. In fact, after a certain threshold, any increase in the input power degrades the performance of the system due to increasing distortion. Another observation from this figure is that increasing the number of transmit antennas always leads to higher spectral efficiency for a fixed transmit power (even at high P).

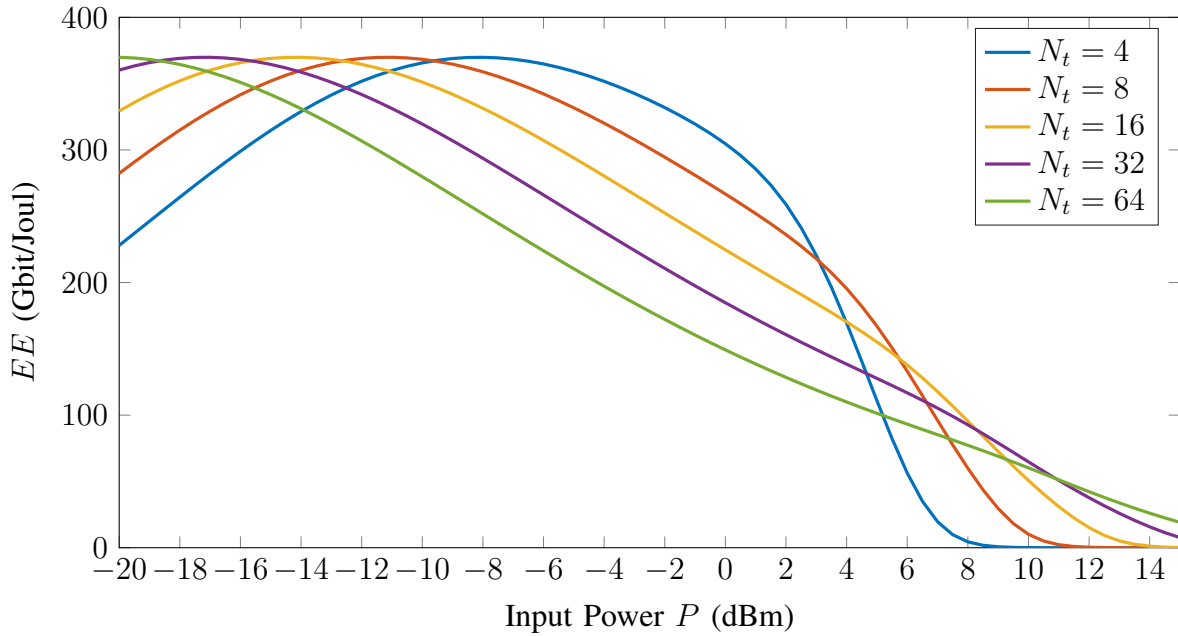


Fig. 6: Energy efficiency of the system in (Gbit/Joul) with varying input power and number of transmit antennas.

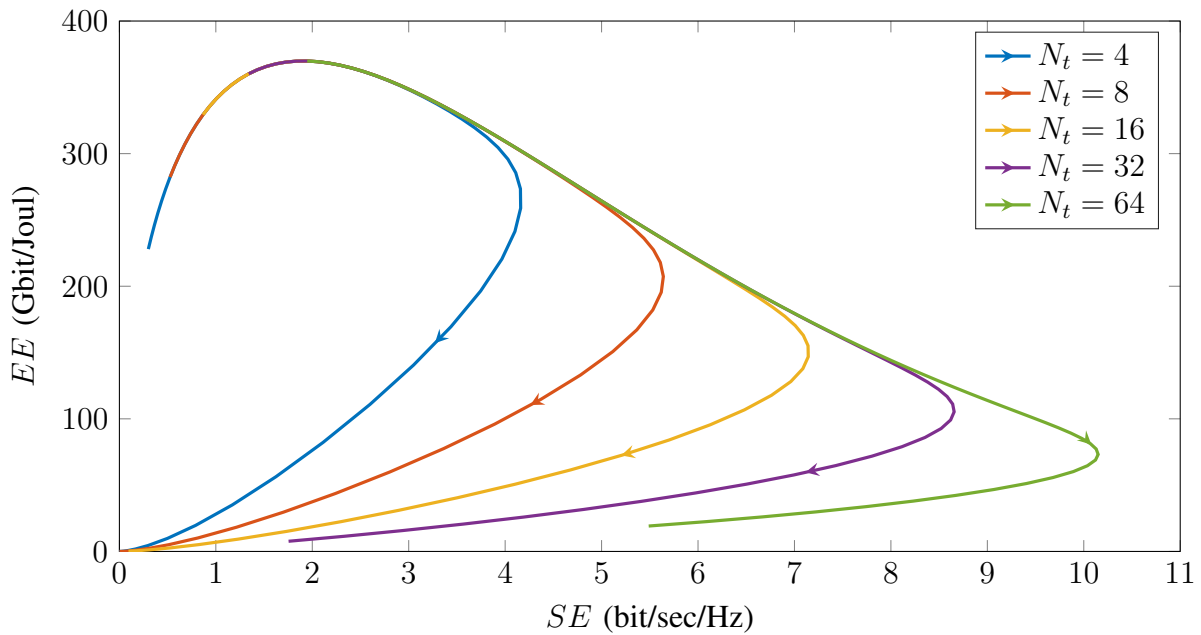


Fig. 7: System energy efficiency vs. spectral efficiency. The input power, P , increases in the direction of arrows.

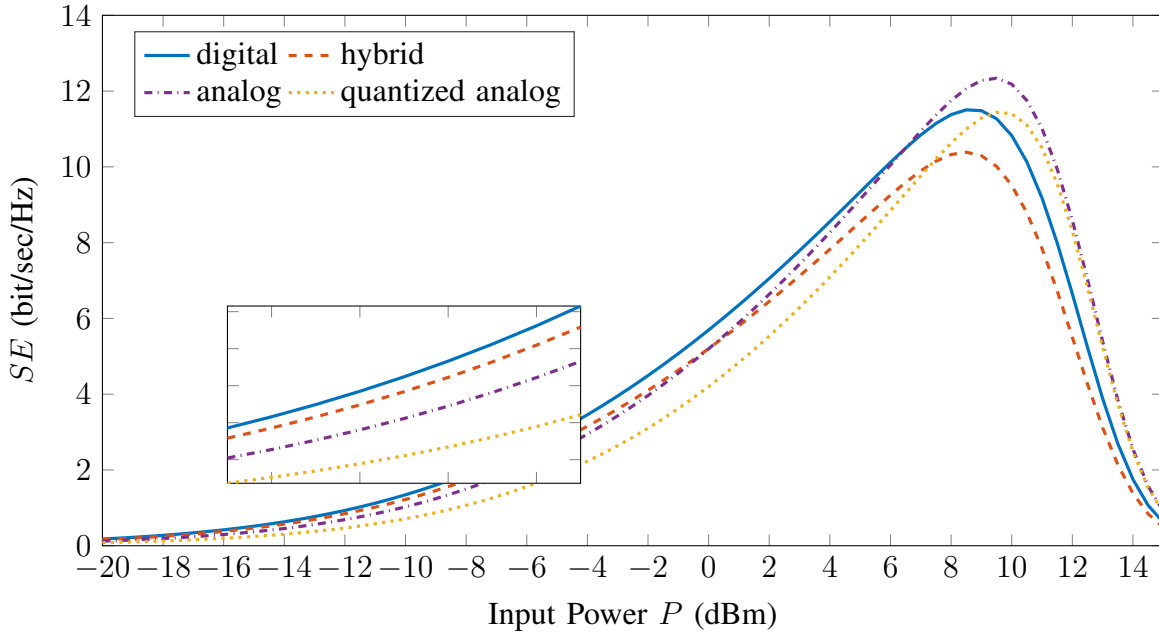
Fig. 6 illustrates the energy efficiency of the system described in Section II versus the input power to the amplification stage, P , for various values of N_t . The energy efficiency in this figure is computed using (22). As the figure implies, at low and high input powers, increasing

N_t improves the energy efficiency while at medium values of P , energy efficiency decreases as N_t increases. Another observation from this figure, which might look counter-intuitive, is that the energy efficiency of the system is small when P is large. This is against the common rule of thumb that by increasing the input power to a PA, it will work more efficiently (see the definition of PA efficiency, $\mu(\cdot)$, in (20)). However, we should note that although the PAs are working more efficiently in their nonlinear region they also distort the signal more severely. Hence, part of the radiated power is in fact the distortion signal power which in turn negatively affects the SE and leads to a degradation of the energy efficiency at the system level, i.e., to a degradation of EE (see the definition of EE in (22)).

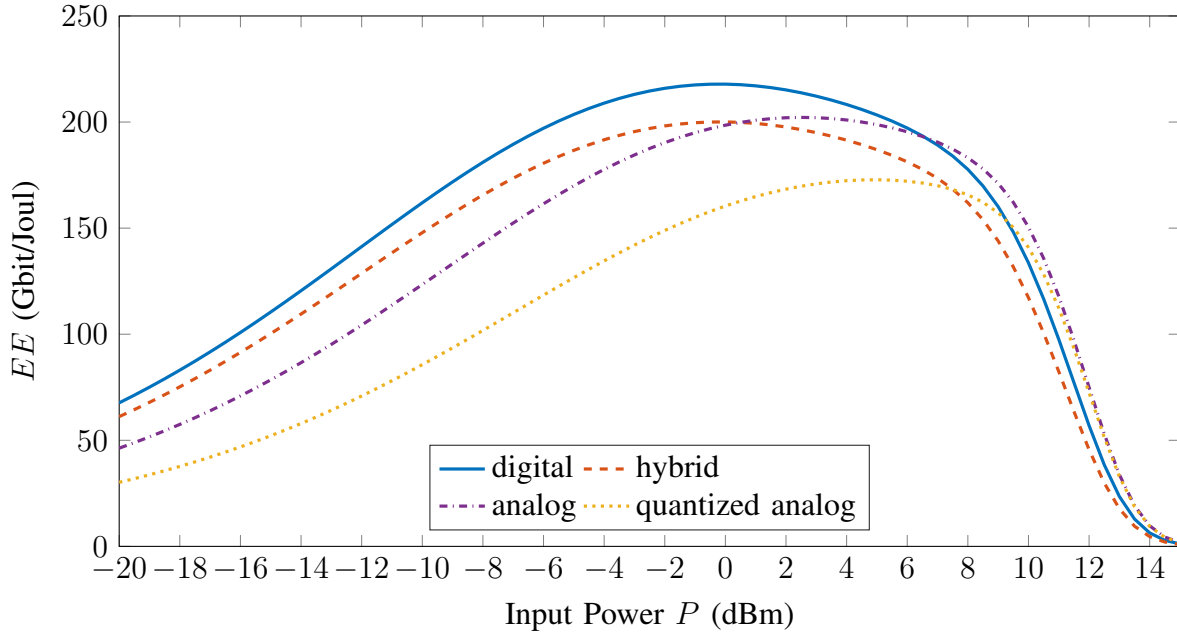
It can clearly be observed from Fig. 5 and Fig. 6 that although the spectral efficiency increases monotonically with power within the whole linear region of the PAs (which can be determined in Fig. 5 by the range of P where curves corresponding to Nonlinear System and Linear System match), EE starts to decline before the PAs enter their nonlinear region. The reason for that will be clear by noting that when $N_{\text{RF}} = 1$ and P/N_t is small using (23) and Corollary 1, the relationship of the system spectral and energy efficiency with the input power can be determined as $\overline{SE} \cong \log_2(1 + \frac{\delta P}{\sigma_n^2})$ and $\overline{EE} \propto \overline{SE}/\sqrt{N_t P}$. This in fact is in line with the results of the previous works, such as the ones in [2] where by considering the consumed power in a linear system (and not only the transmitted power) it is shown that the EE - SE relationship is not always monotonic. The EE - SE relationship is investigated further in Fig. 7.

Fig. 7 illustrates the trade-off between the spectral and energy efficiency in our system. One observation that can be made based on this figure is that, in a system with $N_{\text{RF}} = 1$ RF chain, increasing the number of transmit antennas – although it increases the maximum achievable spectral efficiency – does not affect the maximum energy efficiency of the system significantly. The reason for this can be understood by noting that, as Fig. 6 shows, the energy efficiency for different values of N_t reaches its maximum when P is small and the PAs are working in their linear region. In this region, using Proposition 4, it is straightforward to show that the energy efficiency is related to P and N_t only through their product, $N_t P$. Therefore, for each particular value of N_t there is a corresponding value for P , where $N_t P$ leads to the same optimal energy efficiency. This implies that in a practical system, in order to have a reasonable spectral efficiency and still perform energy efficiently, we should not increase N_t unboundedly.

Fig. 8 shows the spectral and energy efficiency for different beamforming schemes when $N_{\text{RF}} = 5$ and $N_t = 16$. In the digital beamforming scheme, the transmit beamformer is designed



(a) System spectral efficiency.



(b) System energy efficiency.

Fig. 8: System performance for different transmit beamforming schemes.

fully-digital and is matched to the eigen directions of the channel. As the figure illustrates, the digital scheme leads to optimal spectral and energy efficiency when P is small. In the analog beamforming scheme, the baseband beamformer is not used and the RF beamformer is matched to

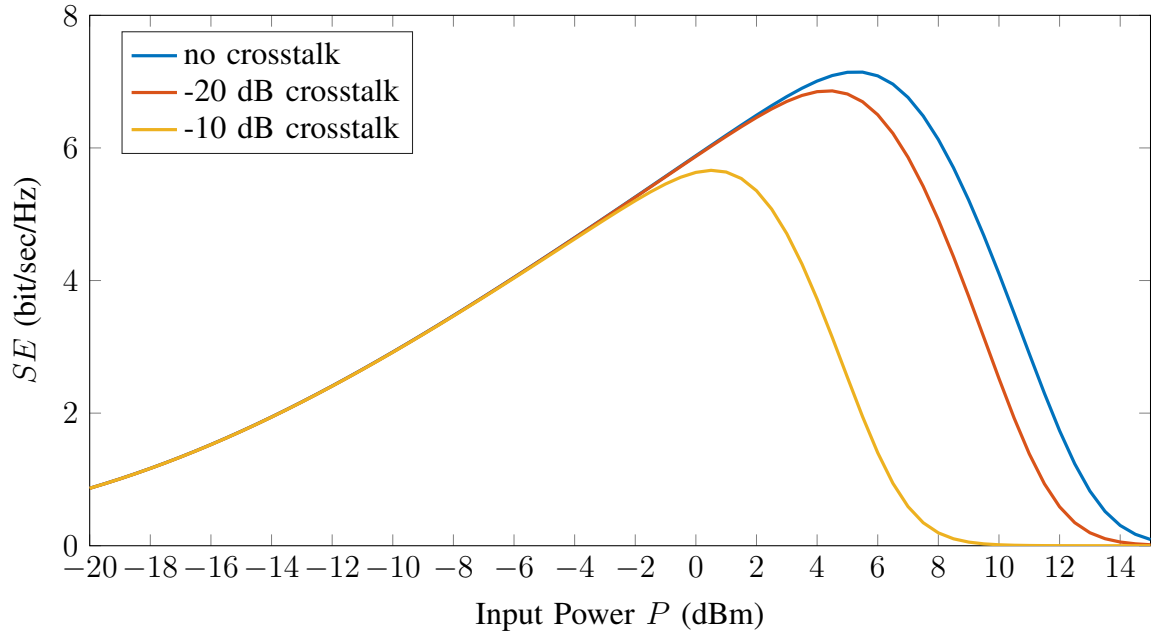
the AoDs of the channel, i.e., $\mathbf{F}_{\text{BB}} = \mathbf{I}_{N_{\text{RF}}}$, and $\mathbf{F}_{\text{RF}} = \mathbf{A}_t$. Observe that the analog beamforming is the optimal beamforming scheme at high P , both in the sense of spectral efficiency and energy efficiency. This is because in this scheme the input power is equally allocated to different PAs and therefore the total radiated distortion power is less compared to the case where the powers are allocated unequally to different PAs (e.g. in the digital beamforming scheme).

In addition to the digital and analog beamforming, the simulation results for a hybrid and a quantized analog beamforming schemes are also plotted in Fig. 8. Both schemes are implemented by revising the MATLAB code used in the simulations of [7]. In both cases, we assume that the full channel state information is available at the transmitter and a 4-bit quantization level is considered for the phase shifters in the analog beamforming stage. The simulation results show that at small P , where the PAs are operating linearly, the hybrid scheme outperforms the analog and quantized analog beamforming schemes. However, at the high input powers, the analog and the quantized analog show a better performance. Again, it is due to the equal power allocation to the different PAs in the analog and the quantized analog schemes.

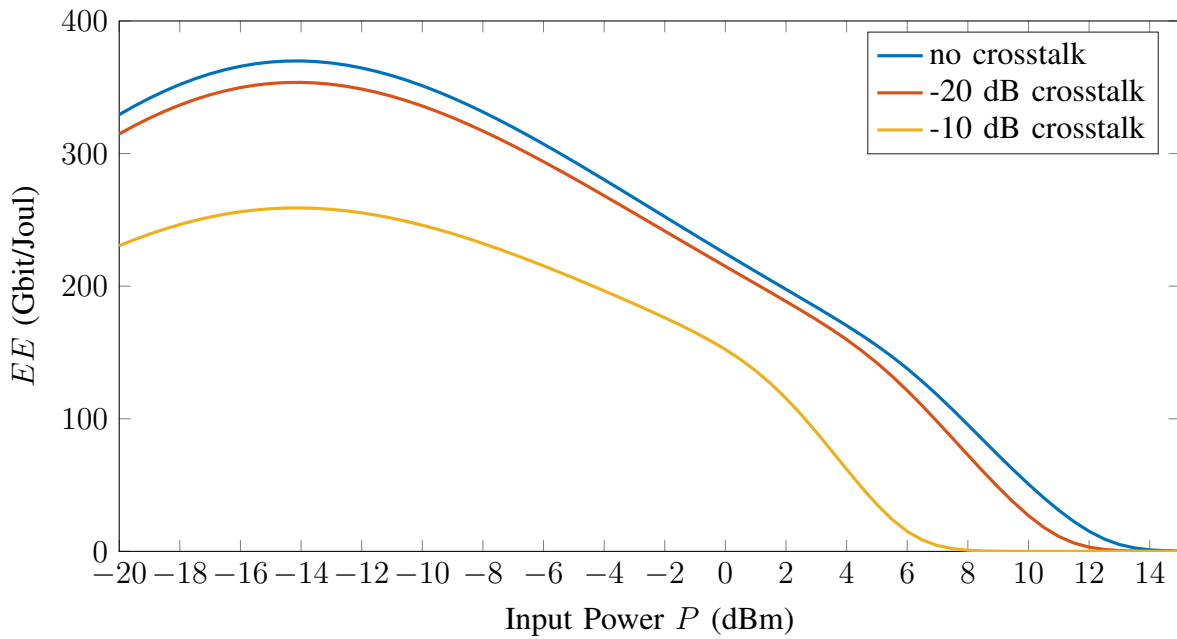
The crosstalk effect in a MIMO system with nonlinear transmit PAs is studied in Fig. 9. In this figure, $N_t = 64$ while the rest of the simulation parameters are the same as the ones in Fig. 5 and Fig. 6. Moreover, the entries of the crosstalk matrix, B_{TX} , are i.i.d. and drawn from the distribution $\mathcal{CN}(0, \sigma_{\text{ct}}^2)$, where σ_{ct}^2 represents the average crosstalk power. In this case, it can be shown that coupling leads to an uneven allocation of the total transmit power in the antenna branches. In other words, unlike the system with no coupling, given a fixed input power $\tilde{P} = \sum_{n=1}^{N_t} \tilde{P}_n$, \tilde{P}_n is not the same for all $n = 1, \dots, N_t$ when crosstalk exists. Therefore, at high \tilde{P} , more distortion power is radiated compared to the case in which the powers are allocated equally to the antenna branches. Fig. 9 shows the spectral efficiency and energy efficiency of the system with different level of crosstalk power. As the figure illustrates, by increasing the crosstalk power, both spectral efficiency and energy efficiency of the system decrease.

VII. CONCLUSIONS

This paper investigated the spectral and energy efficiency of hybrid beamforming for mmWave systems employing nonlinear PAs. In order to capture the impact of nonlinearities on the spectral efficiency, a stochastic model for the transmitted distortion signal was derived. Unlike the models widely-used in the previous works, this model reflects the dependency of the spatial direction of the distortion signal to the spatial direction of the desired signal. Furthermore, a realistic power



(a) System spectral efficiency.



(b) System energy efficiency.

Fig. 9: System performance for different levels of crosstalk power.

consumption model for the transmitter's PAs was considered to find the energy efficiency of the system.

Based on the derived model, we proposed an optimization problem for maximizing the energy

efficiency by designing the beamforming filters. In the special case when the transmitter is equipped with one RF-chain, we found the closed form solutions for the beamforming filters.

Our numerical results show that when using hybrid beamforming, increasing the transmit power level when the number of transmit antennas grows large can be counter-effective in terms of spectral and energy efficiency. On the other hand, with a moderate number of transmit antennas, increasing the transmit power up to a certain threshold is beneficial for the spectral and energy efficiency of the system.

ACKNOWLEDGMENTS

We thank the Associate Editor and the anonymous Reviewers for their insightful comments, which helped to improve the presentation and the contents of the paper.

VIII. APPENDIX: PROOFS

Proof Sketch of Proposition 1

Exploiting (8), the transmitted signal from the n^{th} antenna of the transmitter is $x_n = [\bar{\mathbf{G}}]_{nn} u_n + d_n$. Therefore the average linear gain of the PA of this antenna can be written using the Bussgang theorem [50] as

$$\begin{aligned} [\bar{\mathbf{G}}]_{nn} &\doteq \frac{\mathbb{E}\{x_n u_n^*\}}{\mathbb{E}\{|u_n|^2\}} \stackrel{(a)}{=} \frac{1}{P_n} \mathbb{E} \left\{ \sum_{m=0}^M \beta_{2m+1} |u_n|^{2m+2} \right\} \\ &= \frac{1}{P_n} \sum_{m=0}^M \beta_{2m+1} \mathbb{E} \{ |u_n|^{2m+2} \}, \end{aligned} \quad (24)$$

where (a) follows by substituting for x_n from (3) and noting that by definition $\mathbb{E}\{|u_n|^2\} = P_n$. Now, by taking the expectation of the right-hand side over u_n and considering that u_n is a circularly symmetric complex Gaussian distributed random variable with distribution $\mathcal{CN}(0, P_n)$, the proof will be completed.

Proof of Proposition 2

We introduce a new function $\phi_m : \mathbb{C} \mapsto \mathbb{C}$, $\phi_m(a) \doteq |a|^{2m} a$. In order to continue with the proof, first, we need to study the first- and second-order statistics of $\phi_m(a)$ using the *Isserlis' theorem* and the following lemma. For the sake of completeness, we re-state the Isserlis' theorem below.

Theorem 1. *Isserlis' theorem [51]*

If $[a_1, \dots, a_K]^T$ is a zero-mean multivariate normal random vector, then

$$\mathbb{E} \left\{ \prod_{k=1}^K a_k \right\} = \begin{cases} \sum_S \prod_{B_{ij} \in S} \mathbb{E} \{a_i a_j\} & K \text{ is even,} \\ 0 & K \text{ is odd,} \end{cases} \quad (25)$$

where $B_{ij} = \{a_i, a_j\}$ is an arbitrary 2-subset of $\mathcal{A} = \{a_1, \dots, a_K\}$ and S runs through the list of all possible partitions of \mathcal{A} into 2-subsets.

Note that although Isserlis' theorem is originally developed for real-valued random vectors, it can be extended to the case of complex Gaussian variables as well (see [52]).

Lemma 1. *Consider $a \sim \mathcal{CN}(0, \sigma_a^2)$ and $b \sim \mathcal{CN}(0, \sigma_b^2)$. For any $m, n \in \{0, 1, \dots\}$, $\phi_m(a)$ and $\phi_n(b)$ are zero-mean random processes and the cross-correlation between them is*

$$\mathbb{E} \{ \phi_m(a) \phi_n^*(b) \} = \sum_{q=1}^{\min\{m,n\}} \frac{(m+1)!(n+1)!}{q+1} \binom{m}{q} \binom{n}{q} \sigma_a^{2(m-q)} \sigma_b^{2(n-q)} |\rho|^{2q} \rho, \quad (26)$$

where $\rho = \mathbb{E} \{ ab^* \}$.

Proof: Since the number of multiplied Gaussian terms in $\phi_m(a)$ and $\phi_n(b)$ is odd, the zero-mean property of them is proved as an immediate implication of Isserlis' theorem. Now, inspired by the approach in [53], Isserlis' theorem can again be employed to find the cross-correlation between $\phi_m(a)$ and $\phi_n(b)$. First, we define the following set

$$\mathcal{A} \doteq \{ \overbrace{a, \dots, a}^m, \overbrace{a^*, \dots, a^*}^{m+1}, \overbrace{b, \dots, b}^{n+1}, \overbrace{b^*, \dots, b^*}^n \}, \quad (27)$$

which contains the individual elements in the product $\phi_m(a) \phi_n(b)^*$. Now, we form a two-way table out of the elements in \mathcal{A} as,

$$\begin{array}{cc} \overbrace{a \dots a}^{m+1} & \overbrace{a^* \dots a^*}^m \\ \overbrace{b^* \dots b^*}^{n+1} & \overbrace{b \dots b}^n \end{array}. \quad (28)$$

Since a and b are circularly symmetric, the only 2-subsets that lead to non-zero expectations are $\{a, a^*\}$, $\{b, b^*\}$, $\{a, b^*\}$ and $\{a, b\}$. Similar to [53], we refer to the 2-subsets that contain elements from both rows as *hooking* 2-subsets. We observe that any partition S_{nz} leads to non-zero expectation if

- 1) only consists of non-zero 2-subsets,
- 2) has exactly $q + 1$ hooking 2-subsets of the form $\{a, b^*\}$ and q hooking 2-subsets of the form $\{a^*, b\}$, where $q \in \{0, \dots, \min\{m, n\}\}$.

Therefore a non-zero partition, S_{nz} , can be written as

$$S_{\text{nz}} = \left\{ \overbrace{\{a, a^*\}, \dots, \{a, a^*\}}^{m-q}, \overbrace{\{b, b^*\}, \dots, \{b, b^*\}}^{n-q}, \right. \\ \left. \overbrace{\{a, b^*\}, \dots, \{a, b^*\}}^{q+1}, \overbrace{\{a^*, b\}, \dots, \{a^*, b\}}^q \right\}, \quad (29)$$

and subsequently we have

$$\begin{aligned} & \prod_{B_{ij} \in S_{\text{nz}}} \mathbb{E} \{a_i a_j\} \\ &= \mathbb{E} \{a a^*\}^{m-q} \mathbb{E} \{b b^*\}^{n-q} \mathbb{E} \{a b^*\}^{q+1} \mathbb{E} \{a^* b\}^q \\ &= \sigma_a^{2(m-q)} \sigma_b^{2(n-q)} |\rho|^{2q} \rho. \end{aligned} \quad (30)$$

In [53], in a similar setup, it is shown that the number of partitions with the similar blocks as in (30) is equal to $\frac{(m+1)!(n+1)!}{q+1} \binom{m}{q} \binom{n}{q}$. Therefore, summing over all the non-zero partitions of (28) leads to the result in (26). \square

Now, we are ready to prove the proposition. By substituting from (4) and (10) into (9), the distortion at k^{th} antenna can be written as

$$d_k = \sum_{m=0}^M \beta_{2m+1} (\phi_m(u_k) - P_k^m (m+1)! \phi_0(u_k)). \quad (31)$$

Taking the exception of both sides of (31) and applying Lemma 1 proves the zero-mean property of the distortion signals.

Using (31), the cross-correlation between the distortion noise at k th and j th antennas is computed as

$$\begin{aligned} [\mathbf{C}_d]_{kj} &= \mathbb{E} \{d_k d_j^*\} = \sum_{m=1}^M \sum_{n=1}^M \beta_{2m+1} \beta_{2n+1}^* \\ & \left(\mathbb{E} \{ \phi_m(u_k) \phi_n^*(u_j) \} - P_j^n (n+1)! \mathbb{E} \{ \phi_m(u_k) \phi_0^*(u_j) \} \right. \\ & - P_k^m (m+1)! \mathbb{E} \{ \phi_0(u_k) \phi_n^*(u_j) \} \\ & \left. + P_k^m P_j^n (m+1)! (n+1)! \mathbb{E} \{ \phi_0(u_k) \phi_0^*(u_j) \} \right). \end{aligned} \quad (32)$$

Moreover, by the help of Lemma 1, (32) can be further simplified to

$$[\mathbf{C}_d]_{kj} = \sum_{m=1}^M \sum_{n=1}^M \sum_{q=1}^{\min\{m,n\}} \frac{(m+1)!(n+1)!}{q+1} \binom{m}{q} \binom{n}{q} \\ \times \beta_{2m+1} \beta_{2n+1}^* P_k^{(m-q)} P_j^{(n-q)} \left| [\mathbf{C}_u]_{kj} \right|^{2q} [\mathbf{C}_u]_{kj}$$

Finally by noticing that $\sum_{m=1}^M \sum_{n=1}^M \sum_{q=1}^{\min\{m,n\}}$ is equivalent to $\sum_{q=1}^M \sum_{m=q}^M \sum_{n=q}^M$ and introducing a new function $\gamma_m(P_k)$ as in (12), the proof is completed.

Proof of Proposition 3

We use the following two lemmas in the proof of Proposition 3.

Lemma 2. Consider vector $\mathbf{z} \in \mathbb{C}^N$ with constant modulus entries $|z_n| = \sqrt{\alpha}$, $n = 1, \dots, N$ and define $\mathbf{C}_z \doteq \mathbf{z}\mathbf{z}^H$. Then,

$$\overbrace{(\mathbf{C}_z \odot \dots \odot \mathbf{C}_z)}^{(m+1) \text{ times}} \odot \overbrace{(\mathbf{C}_z^T \odot \dots \odot \mathbf{C}_z^T)}^{m \text{ times}} = \alpha^{2m} \mathbf{C}_z. \quad (33)$$

Proof: Note that $[\mathbf{C}_z]_{ij} = z_i z_j$ and $[\mathbf{C}_z^T]_{ij} = z_i^* z_j^*$ for $i, j \in \{1, \dots, N\}$. Therefore the entry ij of the left hand side of (33) can be written as

$$(z_i z_j)^{m+1} (z_i^* z_j^*)^m = |z_i|^{2m} |z_j|^{2m} z_i z_j \\ = \alpha^{2m} z_i z_j \\ = \alpha^{2m} [\mathbf{C}_z]_{ij}. \quad (34)$$

This completes the proof. \square

Lemma 3. Define the function $f : \mathbb{S}^N \mapsto \mathbb{R}^+$ as

$$f(\mathbf{Z}) \doteq \log_2 \det (\mathbf{I} + (\alpha_2 \mathbf{Z} + \mathbf{I})^{-1} \alpha_1 \mathbf{Z}). \quad (35)$$

For any $\mathbf{Z}' \succeq \mathbf{Z}$ (that is when $\mathbf{Z}' - \mathbf{Z}$ is a PSD matrix), we have $f(\mathbf{Z}') \geq f(\mathbf{Z})$.

Proof: Let us denote the ordered eigenvalues of \mathbf{Z} and \mathbf{Z}' by $\lambda_1 \geq \dots \geq \lambda_N$ and $\lambda'_1 \geq \dots \geq \lambda'_N$, respectively. Since $\mathbf{Z}' \succeq \mathbf{Z}$, we know that $\lambda'_n \geq \lambda_n$ for $n = 1, \dots, N$. Moreover, note that $f(\mathbf{Z})$ can alternatively be expressed as

$$f(\mathbf{Z}) = \sum_{n=1}^N \log_2 \left(1 + \frac{\alpha_1 \lambda_n}{\alpha_2 \lambda_n + 1} \right). \quad (36)$$

Now, by considering that $\log_2(1 + \frac{\alpha_1 \lambda_n}{\alpha_2 \lambda_n + 1})$ is a non-decreasing function of λ_n , we can conclude that $f(\mathbf{Z}') \geq f(\mathbf{Z})$. \square

Observe that when $N_{\text{RF}} = 1$, $\mathbf{C}_{\mathbf{u}} = P \mathbf{F}_{\text{RF}} \mathbf{F}_{\text{RF}}^{\text{H}}$, and \mathbf{F}_{RF} is a vector with constant modulus entries where $|[\mathbf{F}_{\text{RF}}]_n| = \sqrt{1/N_t}$, for $n \in \{1, \dots, N_t\}$. Therefore, the input powers to all the PAs are equal, i.e., $[\mathbf{C}_{\mathbf{u}}]_{11} = P_1 = \dots = P_{N_t} = [\mathbf{C}_{\mathbf{u}}]_{N_t N_t} = P/N_t$. Hence, using Proposition 1, we can show that

$$\bar{\mathbf{G}} = \bar{g} \left(\frac{P}{N_t} \right) \mathbf{I}_{N_t}, \quad (37)$$

and therefore

$$\tilde{\mathbf{C}}_{\mathbf{u}} = \bar{g}_s \left(\frac{P}{N_t} \right) P \mathbf{F}_{\text{RF}} \mathbf{F}_{\text{RF}}^{\text{H}}. \quad (38)$$

Moreover, using Proposition 2 and Lemma 2, it is straightforward to show that in this case

$$\mathbf{C}_{\mathbf{d}} = \bar{g}_d \left(\frac{P}{N_t} \right) P \mathbf{F}_{\text{RF}} \mathbf{F}_{\text{RF}}^{\text{H}}. \quad (39)$$

This implies that the covariance matrices of the transmitted desired signal and distortion signal are equal up to a scaling factor and therefore the signals always have the same spatial direction.

By replacing α_1 and α_2 in (35) with $P/\sigma_n^2 \bar{g}_s(P/N_t)$ and $P/\sigma_n^2 \bar{g}_d(P/N_t)$, respectively, we can show that $SE = f(\mathbf{H}\mathbf{C}_{\mathbf{u}}\mathbf{H}^{\text{H}})$, for $f(\cdot)$ defined in Lemma 3. Hence by considering that $\mathbf{H}\mathbf{C}_{\mathbf{u}}\mathbf{H}^{\text{H}} \preceq P\tilde{\mathbf{H}}\tilde{\mathbf{H}}^{\text{H}}$ for any $\mathbf{C}_{\mathbf{u}} = P\mathbf{F}_{\text{RF}}\mathbf{F}_{\text{RF}}^{\text{H}}$ which satisfies the power constraint $\text{tr}(\mathbf{C}_{\mathbf{u}}) \leq P$ and using Lemma 3, it is straightforward to show that the maximum spectral efficiency in this case is

$$\overline{SE} = f(P\tilde{\mathbf{H}}\tilde{\mathbf{H}}^{\text{H}}), \quad (40)$$

which completes the proof.

Proof of Corollary 1

The following lemma will be used in the proof of this corollary.

Lemma 4. Consider function $h : \mathcal{X} \mapsto \mathbb{R}^+$, where $\mathcal{X} = \{(\mathbf{Z}, \mathbf{r}) \in (\mathbb{S}^N, \mathbb{C}^N) | \mathbf{r}^{\text{H}}\mathbf{r} = 1\}$ and

$$h(\mathbf{Z}, \mathbf{r}) \doteq \log_2 \left(1 + \frac{\alpha_1 \mathbf{r}^{\text{H}} \mathbf{Z} \mathbf{r}}{\alpha_2 \mathbf{r}^{\text{H}} \mathbf{Z} \mathbf{r} + 1} \right). \quad (41)$$

then the following inequality always holds

$$f(\mathbf{Z}) \geq h(\mathbf{Z}, \mathbf{r}), \quad (42)$$

where $f(\mathbf{Z})$ is defined in Lemma 3. Equality holds if and only if \mathbf{Z} is rank one and \mathbf{r} matches the eigenvector of \mathbf{Z} corresponding to its non-zero eigenvalue.

Proof: Define the ordered eigenvalues of \mathbf{Z} as $\lambda_1 \geq \dots \geq \lambda_N$. From [54], we know that

$$\mathbf{r}^H \mathbf{Z} \mathbf{r} \leq \max_{\tilde{\mathbf{r}}} \tilde{\mathbf{r}}^H \mathbf{Z} \tilde{\mathbf{r}} = \lambda_1. \quad (43)$$

Therefore, by noticing that $\log_2 \left(1 + \frac{\alpha_1 \lambda_n}{1 + \alpha_2 \lambda_n} \right)$ is a non-decreasing function of λ_n , we can write

$$\begin{aligned} h(\mathbf{Z}, \mathbf{r}) &\leq \log_2 \left(1 + \frac{\alpha_1 \lambda_1}{\alpha_2 \lambda_1 + 1} \right) \\ &\leq \sum_{n=1}^N \log_2 \left(1 + \frac{\alpha_1 \lambda_n}{\alpha_2 \lambda_n + 1} \right) \\ &\stackrel{(a)}{=} f(\mathbf{Z}), \end{aligned} \quad (44)$$

where (a) is due to Lemma 3.

When \mathbf{Z} is rank-one, then $\lambda_n = 0, \forall n > 1$ and therefore the second inequality in (44) holds with equality. Furthermore, when \mathbf{r} is the eigenvector of \mathbf{Z} corresponding to its non-zero eigenvalue then $\mathbf{r}^H \mathbf{Z} \mathbf{r} = \lambda_1$ and the first inequality holds also with equality. This concludes the proof. \square

Proof of Proposition 4

First, we observe that the optimization variables \mathbf{F}_{RF} and \mathbf{F}_{BB} are coupled neither in the objective function nor in the constraints of the optimization problem (P1). Therefore the optimal solution can be found by first solving (P1) for \mathbf{F}_{RF} and then solving it for \mathbf{F}_{BB} .

Furthermore, we notice that when $N_s = 1$ the baseband beamformer \mathbf{F}_{BB} simplifies to the scalar input power P as was shown in the proof of Proposition 3, the input power, independent from the beamforming filter, is equally divided between the PAs. That is $P_1 = \dots = P_{N_t} = P/N_t$. Therefore, using (21), for $n = 1, \dots, N_t$, we have

$$\bar{P}_{\text{cons},n} = \eta_{\text{max}} \sqrt{P_{\text{max}} P / N_t (\bar{g}_s(P/N_t) + \bar{g}_d(P/N_t))}. \quad (45)$$

Now, we can continue with the proof. Utilizing (22), (P1) is equivalent to the following problem

$$\begin{aligned}
& \underset{\mathbf{F}_{\text{RF}}, \mathbf{F}_{\text{BB}}}{\text{maximize}} && \frac{SE}{P_{\text{cons}}} \\
& \text{subject to} && P_{\text{cons}} \leq P_0 \\
& && |[\mathbf{F}_{\text{RF}}]_{i,j}| = \sqrt{1/N_t}, \quad \forall i, j \\
& \underline{(a)} \underset{\mathbf{F}_{\text{BB}}}{\text{maximize}} && \frac{\overline{SE}}{P_{\text{cons}}} \\
& \text{subject to} && P_{\text{cons}} \leq P_0,
\end{aligned} \tag{46}$$

where (a) follows by noting that \mathbf{F}_{RF} , \mathbf{F}_{BB} are uncoupled and using Proposition 3. Since $N_s = 1$, we can replace \mathbf{F}_{BB} by P in (46) and P_{cons} by $\overline{P}_{\text{cons}} = \sum_{n=1}^{N_t} \overline{P}_{\text{cons},n}$. This concludes the proof.

REFERENCES

- [1] E. G. Larsson, O. Edfors, F. Tufvesson, and T. L. Marzetta, "Massive MIMO for next generation wireless systems," *IEEE Commun. Mag.*, vol. 52, no. 2, pp. 186–195, Feb. 2014.
- [2] S. Han, C. I. I, Z. Xu, and C. Rowell, "Large-scale antenna systems with hybrid analog and digital beamforming for millimeter wave 5G," *IEEE Commun. Mag.*, vol. 53, no. 1, pp. 186–194, Jan. 2015.
- [3] S. Rangan, T. S. Rappaport, and E. Erkip, "Millimeter-wave cellular wireless networks: Potentials and challenges," *Proc. IEEE*, vol. 102, no. 3, pp. 366–385, Mar. 2014.
- [4] Z. Pi and F. Khan, "An introduction to millimeter-wave mobile broadband systems," *IEEE Communications Magazine*, vol. 49, no. 6, pp. 101–107, 2011.
- [5] S. Hur, T. Kim, D. J. Love, J. V. Krogmeier, T. A. Thomas, and A. Ghosh, "Millimeter wave beamforming for wireless backhaul and access in small cell networks," *IEEE Trans. Commun.*, vol. 61, no. 10, pp. 4391–4403, Oct. 2013.
- [6] O. E. Ayach, S. Rajagopal, S. Abu-Surra, Z. Pi, and R. W. Heath, "Spatially sparse precoding in millimeter wave MIMO systems," *IEEE Trans. Wireless Commun.*, vol. 13, no. 3, pp. 1499–1513, Mar. 2014.
- [7] A. Alkhateeb, O. E. Ayach, G. Leus, and R. W. Heath, "Channel estimation and hybrid precoding for millimeter wave cellular systems," *IEEE J. Sel. Top. Signal Process.*, vol. 8, no. 5, pp. 831–846, Oct. 2014.
- [8] S. Kutty and D. Sen, "Beamforming for millimeter wave communications: An inclusive survey," *IEEE Communications Surveys Tutorials*, vol. 18, no. 2, pp. 949–973, Sep. 2016.
- [9] S. Noh, M. D. Zoltowski, and D. J. Love, "Training sequence design for feedback assisted hybrid beamforming in massive MIMO systems," *IEEE Trans. Commun.*, vol. 64, no. 1, pp. 187–200, Jan. 2016.
- [10] J. Song, J. Choi, and D. J. Love, "Common codebook millimeter wave beam design: Designing beams for both sounding and communication with uniform planar arrays," *IEEE Trans. Commun.*, vol. 65, no. 4, pp. 1859–1872, Apr. 2017.
- [11] S. He, J. Wang, Y. Huang, B. Ottersten, and W. Hong, "Codebook-based hybrid precoding for millimeter wave multiuser systems," *IEEE Trans. Signal Process.*, vol. 65, no. 20, pp. 5289–5304, Oct. 2017.
- [12] H. Shokri-Ghadikolaei, F. Boccardi, C. Fischione, G. Fodor, and M. Zorzi, "Spectrum sharing in mmWave cellular networks via cell association, coordination, and beamforming," *IEEE J. Sel. Areas Commun.*, vol. 34, no. 11, pp. 2902–2917, Nov. 2016.
- [13] C. Studer, M. Wenk, and A. Burg, "MIMO transmission with residual transmit-RF impairments," in *Proc. Int. ITG Workshop Smart Antennas (WSA)*, Feb. 2010, pp. 189–196.

- [14] J. Qi and S. Aissa, "Analysis and compensation of power amplifier nonlinearity in MIMO transmit diversity systems," *IEEE Trans. Veh. Technol.*, vol. 59, no. 6, pp. 2921–2931, July 2010.
- [15] C. Studer, M. Wenk, and A. Burg, "System-level implications of residual transmit-RF impairments in MIMO systems," in *Proc. 5th European Conf. Antennas and Propagation (EUCAP)*, Apr. 2011, pp. 2686–2689.
- [16] E. Björnson, P. Zetterberg, and M. Bengtsson, "Optimal coordinated beamforming in the multicell downlink with transceiver impairments," in *Proc. IEEE Global Communications Conf. (GLOBECOM)*, Dec. 2012, pp. 4775–4780.
- [17] F. M. Ghannouchi and O. Hammi, "Behavioral modeling and predistortion," *IEEE Microwave Mag.*, vol. 10, no. 7, pp. 52–64, Dec. 2009.
- [18] J. Qi and S. Aissa, "On the power amplifier nonlinearity in MIMO transmit beamforming systems," *IEEE Trans. Commun.*, vol. 60, no. 3, pp. 876–887, March 2012.
- [19] S. V. Zavjalov, D. K. Fadeev, and S. V. Volvenko, "Influence of input power backoff of nonlinear power amplifier on BER performance of optimal SEFDM signals," in *8th International Congress on Ultra Modern Telecommunications and Control Systems and Workshops (ICUMT)*, 2016.
- [20] T. Schenk, *RF imperfections in high-rate wireless systems: impact and digital compensation*. Springer Science & Business Media, 2008.
- [21] J.-A. Lucciardi, N. Thomas, M.-L. Boucheret, C. Poulliat, and G. Mesnager, "Trade-off between spectral efficiency increase and papr reduction when using ftn signaling: Impact of non linearities," in *IEEE International Conference on Communications (ICC)*, 2016.
- [22] H. Ochiai, "An analysis of band-limited communication systems from amplifier efficiency and distortion perspective," *IEEE Trans. Commun.*, vol. 61, no. 4, pp. 1460–1472, Apr. 2013.
- [23] E. Björnson, P. Zetterberg, M. Bengtsson, and B. Ottersten, "Capacity limits and multiplexing gains of MIMO channels with transceiver impairments," *IEEE Commun. Lett.*, vol. 17, no. 1, pp. 91–94, Jan. 2013.
- [24] E. Björnson, J. Hoydis, M. Kountouris, and M. Debbah, "Massive MIMO systems with non-ideal hardware: Energy efficiency, estimation, and capacity limits," *IEEE Trans. Inf. Theory*, vol. 60, no. 11, pp. 7112–7139, Nov. 2014.
- [25] E. Björnson, M. Bengtsson, and B. Ottersten, "Optimal multiuser transmit beamforming: A difficult problem with a simple solution structure [lecture notes]," *IEEE Signal. Proc. Mag.*, vol. 31, no. 4, pp. 142–148, July 2014.
- [26] R. Brandt, E. Björnson, and M. Bengtsson, "Weighted sum rate optimization for multicell MIMO systems with hardware-impaired transceivers," in *Proc. Acoustics, Speech and Signal Processing (ICASSP) 2014 IEEE International Conference on*, May 2014, pp. 479–483.
- [27] N. N. Moghadam, P. Zetterberg, P. Händel, and H. Hjalmarsson, "Correlation of distortion noise between the branches of MIMO transmit antennas," in *Proc. Indoor and Mobile Radio Communications - (PIMRC) 2012 IEEE 23rd Int. Symp. Personal*, Sep. 2012, pp. 2079–2084.
- [28] E. Björnson and E. Jorswieck, "Optimal resource allocation in coordinated multi-cell systems," *Foundations and Trends® in Communications and Information Theory*, vol. 9, no. 2-3, 2013.
- [29] E. Björnson, L. Sanguinetti, J. Hoydis, and M. Debbah, "Optimal design of energy-efficient multi-user MIMO systems: Is massive MIMO the answer?" *IEEE Trans. Wireless Commun.*, vol. 14, no. 6, pp. 3059–3075, June 2015.
- [30] M. Sabbaghian, A. I. Sulyman, and V. Tarokh, "Analysis of the impact of nonlinearity on the capacity of communication channels," *IEEE Trans. Inf. Theory*, vol. 59, no. 11, pp. 7671–7683, Nov 2013.
- [31] M. Fozooni, M. Matthaiou, E. Björnson, and T. Q. Duong, "Performance limits of MIMO systems with nonlinear power amplifiers," in *Proc. 2015 IEEE Global Communications Conference (GLOBECOM)*, Dec 2015, pp. 1–7.
- [32] M. Wu, D. Wuebben, A. Dekorsy, P. Baracca, V. Braun, and H. Halbauer, "Hardware impairments in millimeter wave

- communications using OFDM and SC-FDE,” in *Proc. Smart Antennas (WSA), 2016 International ITG Workshop on*, March 2016, pp. 1–8.
- [33] A. Khansefid, H. Minn, Q. Zhan, N. Al-Dhahir, H. Huang, and X. Du, “Waveform parameter design and comparisons for millimeter-wave massive MIMO systems with RF distortions,” in *Proc. IEEE Globecom Workshops (GC Wkshps)*, Dec 2016, pp. 1–6.
- [34] H. Yan and D. Cabric, “Digital predistortion for hybrid precoding architecture in millimeter-wave massive MIMO systems,” in *Proc. 42nd IEEE Int. Conf. on Acoustics, Speech and Signal Process.*, Mar. 2017.
- [35] D. Persson, T. Eriksson, and E. G. Larsson, “Amplifier-aware multiple-input multiple-output power allocation,” *IEEE Communications Letters*, vol. 17, no. 6, pp. 1112–1115, June 2013.
- [36] —, “Amplifier-aware multiple-input single-output capacity,” *IEEE Trans. Commun.*, vol. 62, no. 3, pp. 913–919, March 2014.
- [37] D. Ying, D. J. Love, and B. M. Hochwald, “Closed-loop precoding and capacity analysis for multiple-antenna wireless systems with user radiation exposure constraints,” *IEEE Trans. Wireless Commun.*, vol. 14, no. 10, pp. 5859–5870, Oct. 2015.
- [38] —, “Sum-rate analysis for multi-user MIMO systems with user exposure constraints,” *IEEE Trans. Wireless Commun.*, vol. 16, no. 11, pp. 7376–7388, Nov. 2017.
- [39] M. R. Castellanos, D. J. Love, and B. M. Hochwald, “Hybrid precoding for millimeter wave systems with a constraint on user electromagnetic radiation exposure,” in *2016 50th Asilomar Conference on Signals, Systems and Computers*, Nov. 2016, pp. 296–300.
- [40] C. Mollén, E. G. Larsson, and T. Eriksson, “Waveforms for the massive MIMO downlink: Amplifier efficiency, distortion and performance,” *IEEE Trans. Commun.*, vol. 64, no. 12, pp. 5050 – 5063, Dec. 2016.
- [41] R. Mendez-Rial, C. Rusu, N. Gonzalez-Prelcic, A. Alkhateeb, and R. W. Heath, “Hybrid MIMO architectures for millimeter wave communications: Phase shifters or switches?” *IEEE Access*, vol. 4, pp. 247–267, 2016.
- [42] P. B. Kenington, *High-Linearity RF Amplifier Design*. Artech House Publishers, 2000.
- [43] S. C. Cripps, *Advanced Techniques in RF Power Amplifier Design*. Artech House Publishers, 2002.
- [44] C. Mollén, U. Gustavsson, T. Eriksson, and E. G. Larsson. (2017, Nov.) Spatial characteristics of distortion radiated from antenna arrays with transceiver nonlinearities. [Online]. Available: <http://arxiv.org/abs/1711.02439>
- [45] M. R. Akdeniz, Y. Liu, M. K. Samimi, S. Sun, S. Rangan, T. S. Rappaport, and E. Erkip, “Millimeter wave channel modeling and cellular capacity evaluation,” *IEEE J. Sel. Areas Commun.*, vol. 32, no. 6, pp. 1164–1179, Jun. 2014.
- [46] D. Dardari, V. Tralli, and A. Vaccari, “A theoretical characterization of nonlinear distortion effects in OFDM systems,” *IEEE Trans. Commun.*, vol. 48, no. 10, pp. 1755–1764, Oct. 2000.
- [47] O. Raaesi, A. Gokceoglu, P. C. Sofotasios, M. Renfors, and M. Valkama, “Modeling and estimation of massive mimo channel non-reciprocity: Sparsity-aided approach,” in *2017 25th European Signal Processing Conference (EUSIPCO)*, Aug 2017, pp. 2596–2600.
- [48] A. J. Goldsmith and P. P. Varaiya, “Capacity of fading channels with channel side information,” *IEEE Trans. Inf. Theory*, vol. 43, no. 6, pp. 1986–1992, Nov. 1997.
- [49] M. Faulkner and T. Mattsson, “Spectral sensitivity of power amplifiers to quadrature modulator misalignment,” *IEEE Trans. Veh. Technol.*, vol. 41, no. 4, pp. 516–525, Nov 1992.
- [50] J. J. Bussgang, “Crosscorrelation function of amplitude-distorted Gaussian signals,” Research Lab. Electron, M.I.T., Cambridge, MA, Tech. Rep. 216, March 1952.
- [51] L. Isserlis, “On a formula for the product-moment coefficient of any order of a normal frequency distribution in any number of variables,” *Biometrika*, vol. 12, no. 1/2, pp. 134–139, 1918.

- [52] I. Reed, "On a moment theorem for complex gaussian processes," *IRE Transactions on Information Theory*, vol. 8, no. 3, pp. 194–195, April 1962.
- [53] G. T. Zhou and R. Raich, "Spectral analysis of polynomial nonlinearity with applications to RF power amplifiers," *EURASIP Journal on Advances in Signal Processing*, vol. 2004, no. 12, p. 1, Sep. 2004. [Online]. Available: <http://dx.doi.org/10.1155/S1110865704312114>
- [54] R. A. Horn and C. R. Johnson, *Matrix analysis*. Cambridge university press, 2012.